Auditory detection is modulated by theta phase of silent lip movements

Emmanuel Biau[1, 2, *], Danying Wang[1, 2], Hyojin Park[1, 2], Ole Jensen[1, 2], Simon Hanslmayr[1, 2].

[1] School of Psychology, University of Birmingham, Edgbaston, Birmingham, UK.

[2] Centre for Human Brain Health, University of Birmingham, Birmingham, UK

CONTACT INFO: e.biau@bham.ac.uk

LEAD CONTACT: Emmanuel Biau

KEYWORDS: Lip movements; theta oscillations; entrainment; auditory processing.

SUMMARY

Audiovisual speech perception relies on our expertise to map a speaker's lip movements with speech sounds. This multimodal matching is facilitated by salient syllable features that align lip movements and acoustic envelope signals in the 4 - 8 Hz theta band (Chandrasekaran et al., 2009). The predominance of theta rhythms in speech processing has been firmly established by studies showing that neural oscillations track the acoustic envelope in the primary auditory cortex (Giraud & Poeppel, 2012). Equivalently, theta oscillations in the visual cortex entrain to lip movements (Park et al., 2016), and the auditory cortex is recruited during silent speech perception (Bourguignon et al., 2020; Cross et al., 2019; Calvert et al., 1997). These findings suggest that neuronal theta oscillations play a functional role in organising information flow across visual and auditory sensory areas. We presented silent speech movies while participants performed a pure tone detection task to test whether entrainment to lip movements enslaves the auditory system and drives behavioural outcomes. We showed that auditory detection varied depending on the ongoing theta phase conveyed by lip movements in the movies. In a complementary experiment presenting the same movies while recording participants' electro-encephalogram (EEG), we found that silent lip movements entrained neural oscillations in the visual and auditory cortices with the visual phase leading the auditory phase. These results support the idea that the visual cortex entrained by lip movements increases the sensitivity of the auditory cortex at relevant time-windows for speech comprehension as a filtering modulator relying on theta phase synchronisation.

RESULTS

When hearing gets difficult, people often visually focus on their interlocutors' mouth to match lip movements with sounds and to improve speech perception. Mouth opening indeed shares common features with auditory speech envelope, which temporally synchronize on dominant 4 - 8 Hz theta rhythms imposed by syllables (Park et al., 2016; Chandrasekaran et al., 2009; Luo & Poeppel, 2007). Neural oscillations in the auditory cortex track the auditory envelope structure during speech perception, suggesting that this "entrainment" reflects signal analysis (Keitel et al., 2018; Pelle & Davis, 2012; Gross et al., 2013; Giraud & Poeppel, 2012). Although the term entrainment is currently under debate

(Meyer, Sun & Martin, 2019; Obleser & Keyser, 2019; Haegens & Zion Golumbic, 2018; Rimmele et al., 2018), here we use it to describe neural patterns tracking salient features conveyed in speech signals which occur at theta frequency (4-8 Hz). Previous studies demonstrated that the visual perception of silent moving lips entrains theta oscillations in the visual cortex and recruits auditory processing regions (Bourguignon et al., 2020; Cross et al., 2019), even in the absence of sound (Cross et al., 2015; Calvert et al., 1997). Further, information specific to lip movements is represented not only in the visual cortex but also in the auditory cortex (Park et al., 2018). These results beg the question of whether visual perception of lip movements modulates the auditory cortex in a functional way. In other words, do purely visually induced theta speech rhythms impose time windows that render the auditory cortex more sensitive to input in a phasic manner? If the answer to this question is yes, then visually focussing on your interlocutor's mouth when you have trouble understanding them would indeed be an effective filter modulator to increase auditory sensitivity.

Entrainment to lip movements during silent speech drives behavioural performance

To address this question, we adapted an auditory tone detection paradigm in which a continuous white noise was presented simultaneously with silent movies displaying speakers engaged in conversations (Figure 1 and STAR Methods). Participants were instructed to press a key as fast and accurate as possible every time when they detected a pure tone (1 kHz, 100 ms) embedded in the white noise at individual threshold (determined with a calibration task). In the condition of interest, there were two target tones: the first tone occurred randomly in the first half of the trial (0 to 2.5 s after trial onset; early window) and the second tone occurred randomly in the second half of the trial (2.5 to 5 s; late window). Two additional conditions containing zero or one single tone were introduced to estimate the false alarm rates (FA) and to reduce the predictability of the second tone by the occurrence of the first one. The three conditions were counterbalanced and randomised across six blocks of 50 trials (100 trials per condition). To test the first hypothesis of visual entrainment affecting auditory processing, participants were asked to attend carefully to the silent movies centred on the speakers' nose displayed with sound albeit non-informative. Crucially, the videos were preselected such that lip movements occurred in the

4 - 8 Hz theta range. We determined at which theta frequency the vertical mouth's apertures and auditory speech envelope showed significant dependencies in the original clips by using mutual information method (see STAR Methods). This paradigm allowed us to link directly the onset of detected tones with the phase of the ongoing theta activity conveyed by the lip movements. As neural entrainment increases over time (Thut et al., 2011; Hanslmayr, Axmacher & Inman, 2019), we compared behavioural performance between the early and late time-windows (containing respectively the first and second tones).

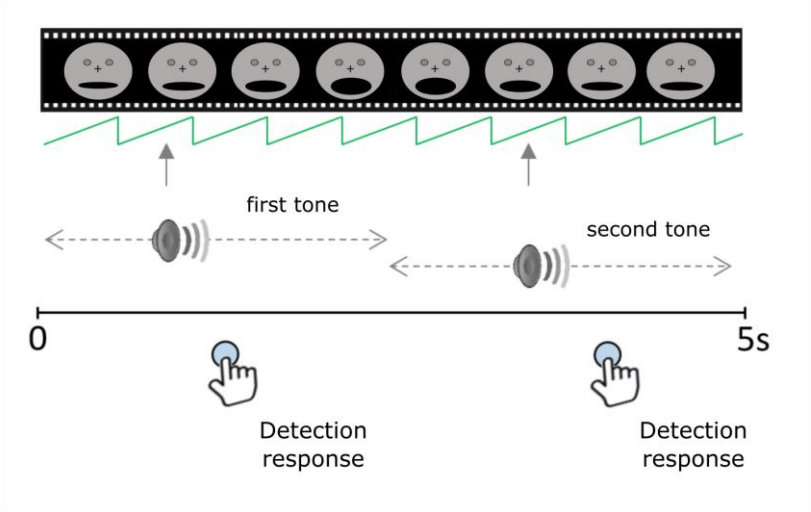

Figure 1: Experimental Paradigm of the Tone Detection Task (TDT). For each trial, continuous white noise and a silent movie were presented together during five seconds (drawing of a speaking face substituted to illustrate the relevant concept here). A first pure tone occurred randomly in the first half of the trial while a second tone occurred randomly in the second half of the trial. Participants were instructed to respond as fast and accurately as possible whenever they detected a tone. In the one tone condition, the white noise track contained only one tone that occurred randomly between the two halves of the trial. In the zero tone condition, the sound of the trial contained only white noise. The green line represents the ongoing theta phase conveyed by lip movements.

We compared the mean theta phase distributions between first and second tones' onsets across participants (Figure 2A; see STAR Methods). For each participant, the corresponding theta phases in ongoing lip activity at detected first and second tone onsets were averaged across hit trials. Individual mean theta phases were then averaged across subjects to

estimate phase locking of hits to the theta signal conveyed visually in the first and second tone time-windows. Two Rayleigh's uniformity tests were performed on the first and second grand average theta phase distributions separately. For the first tone window, the Rayleigh's test did not reject the hypothesis of uniform distribution (n = 24; μ = 1.944 rad or 111.384°; r = 0.282; p = 0.148, Bonferroni-corrected). In contrast, the Rayleigh's test revealed that mean phases were not uniformly distributed in the second tone window (n = 24; μ = -0.999 rad or 302.763°; r = 0.44; p < 0.01, Bonferroni-corrected). Further, a permutation test was performed on the resultant vector length (r) difference between the first and second tones to test whether the strength of visual entrainment in the second tone window was significantly stronger than in the first tone window, which indeed was the case (permutations: 10,000; effect size = 0.158; p = 0.015; Figure 2A; see STAR Methods). We performed two additional permutation tests on resultant vector length difference between hits and misses in the first and second tone windows separately to test that visual entrainment related to successful auditory processing. No significant difference of vector length was found in the first tone window (permutations: 10,000; effect size = 0.041; p = 0.405), whereas in the second tone window the resultant hits vector strongly tended to be longer than the misses vector (permutations: 10,000; effect size = 0.228; p = 0.052).

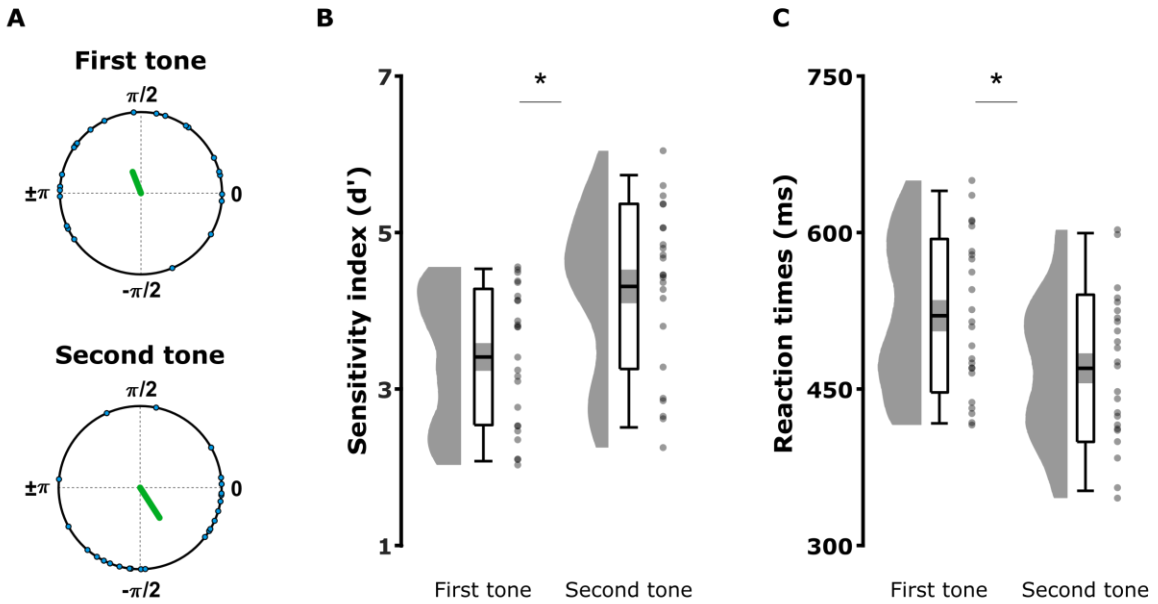

Figure 2: Visual entrainment and tone detection performance in the two tones condition. (A) Resultant r vector length (green line) from grand average phase at the onsets of

correctly detected first and second tones across participants. The individual mean theta phases are depicted in polar coordinates (blue circles). (B) Mean sensitivity index (d' = $Z_{Hit\ rate}$ - $Z_{FA\ rate}$) and (C) reaction times of first and second tone hits. The graphs depict the density, the grand average (mean ± standard error of the mean; errors bars: 95 % confidence interval), and individual means (grey dots) for first/second tones. Significant contrasts are evidenced with stars ($p < 0.05$).

Following up, we investigated whether tone detection differed between the first and second tones windows. Such a difference might reflect an auditory bias by visual inputs (Figure 2B). First, two independent one-sample t-tests established that participants detected the first and second tones in the two tones condition, as the d' scores were greater than zero (first tone: $T(1,23) = 20.014$; $p < 0.001$, two-tailed; second tone: $T(1,23) = 21.124$; $p < 0.001$, two-tailed). Second, a paired-samples t-test confirmed that the second tones were better detected than the first ones ($T(1, 23) = -4.488$; $p < 0.001$; two-tailed; Fig. 2B). Third, a paired-sample t-test applied on the hit reaction times showed that participants responded faster to second compared to first tones ($T(1, 23) = 5.486$; $p < 0.001$; two-tailed; Figure 2C). Importantly, the improvement of the second tone detection could not be attributed to a simple attentional effect due to the presence of the preceding first one, as the single tone condition replicated the two tones condition performances (i.e. by sorting the single tones as first/second tones according to their onsets; see Figure S1B). Finally, a paired-samples t-test performed on the FA rates in the no tone condition confirmed that detection performance modulations did not reflect a change in response bias between the two windows ($T(1, 23) = 0.627$; $p = 0.537$; two-tailed). Altogether, these results established that entrainment to theta lips activity increased in time and coincided temporally with increases in auditory detection. In the next step, we aimed at establishing whether a potential audiovisual communication relying on the critical theta organisation of information flows was reflected in the brain.

Visual cortex leads synchronization to left auditory cortex via theta oscillations during silent lips perception

The above results suggest that visual speech stimuli may recruit the auditory regions via entrainment to render some time-windows more sensible to auditory detection than others.

To test this hypothesis on a neural level, we recorded the EEG signal of 23 new participants during the perception of the same 60 silent movies used in the previous tone detection task. Participants were instructed to attend to each movie and rate its emotional content based on the speaker's face. The movies were presented in a single block and randomised across participants. First, the sources of interest responding to speakers' lip movements were identified applying a linearly constrained minimum variance beamforming method. Neural entrainment to lip movements was estimated by computing mutual information (MI) on the theta phase between the EEG epochs and corresponding lip signals in the equivalent first (0 to 2.5 s) and second (2.5 to 5 s) tone windows. Just as in the behavioural data, we assessed whether entrainment increased over time by contrasting the difference of MI between the first and second time window. Second, the EEG data at the identified visual and auditory sources were reconstructed to perform single-trial phase coupling analysis. The synchrony between visual and auditory sources was reflected by the distribution of theta phase angle differences $\phi_{A\text{-}V} = \phi_{audio} - \phi_{visual}$ at each time-point within the first and second tone windows, and the directionality of the coupling was evidenced with the sign of $\phi_{A\text{-}V}$ (i.e. a mean distribution of $\phi_{A\text{-}V} = 0$ would mean perfect phase alignment, while $\phi_{A\text{-}V} < 0$ would mean that the visual phase leads the auditory phase; see STAR Methods).

Source localisation analysis revealed that the maximum increases in MI_{second} as compared to MI_{first} were localised in the expected left visual and auditory cortices, as well as in the right visual cortex to a lesser extend (Figure 3A). This result supports the recruitment of both sensory areas during the perception of speakers' lip movements even in the absence of speech sound. Two separate Rayleigh tests confirmed non-uniform distributions of $\phi_{A\text{-}V}$ in the first ($n = 23$; $\mu = -1.99$ rad or -114.45°; $r = 0.768$; $p < 0.001$, Bonferroni-corrected) and second tone windows ($n = 23$; $\mu = -0.92$ rad or -52.79°; $r = 0.875$; $p < 0.001$, Bonferroni-corrected). An additional Kuiper two-sample test confirmed that the mean $\phi_{A\text{-}V}$ distributions between the first and second tone windows converged towards two different preferred angles ($k = 3.614 \times 10^5$; $p < 0.001$). Further, an increase in theta phase synchrony between visual and auditory areas would be reflected by a more consistent distribution of $\phi_{A\text{-}V}$ towards zero degree. To quantify the modulation of phase coupling with entrainment, we computed the resultant vector length r of the distance between the observed $\phi_{A\text{-}V}$ in the data and a fixed zero $\phi_{A\text{-}V}$ in the first and second windows separately (zero $\phi_{A\text{-}V} = 0$; meaning

that visual and auditory theta phases are perfectly aligned with a constant offset of zero at each time-point of the time-window). A paired-samples t-test showed that the resultant vector length r of the distance between the observed ϕ_{A-V} and the zero ϕ_{A-V} was significantly greater in the second tone window ($T(1, 22) = -2.135$; $p = 0.044$; two-tailed), confirming that synchrony between auditory and visual sources improved with time (Figure 3B, C and D). The negative theta phase angle differences ϕ_{A-V} in both the first and second tone windows confirmed that the visual phase led the auditory phase, in line with the idea of visual oscillations responding first to the lips inputs and then enslaving theta oscillations in the auditory cortex. Altogether, these results support our hypothesis that visual cortex led synchronization to left auditory cortex via theta oscillations during silent lips perception.

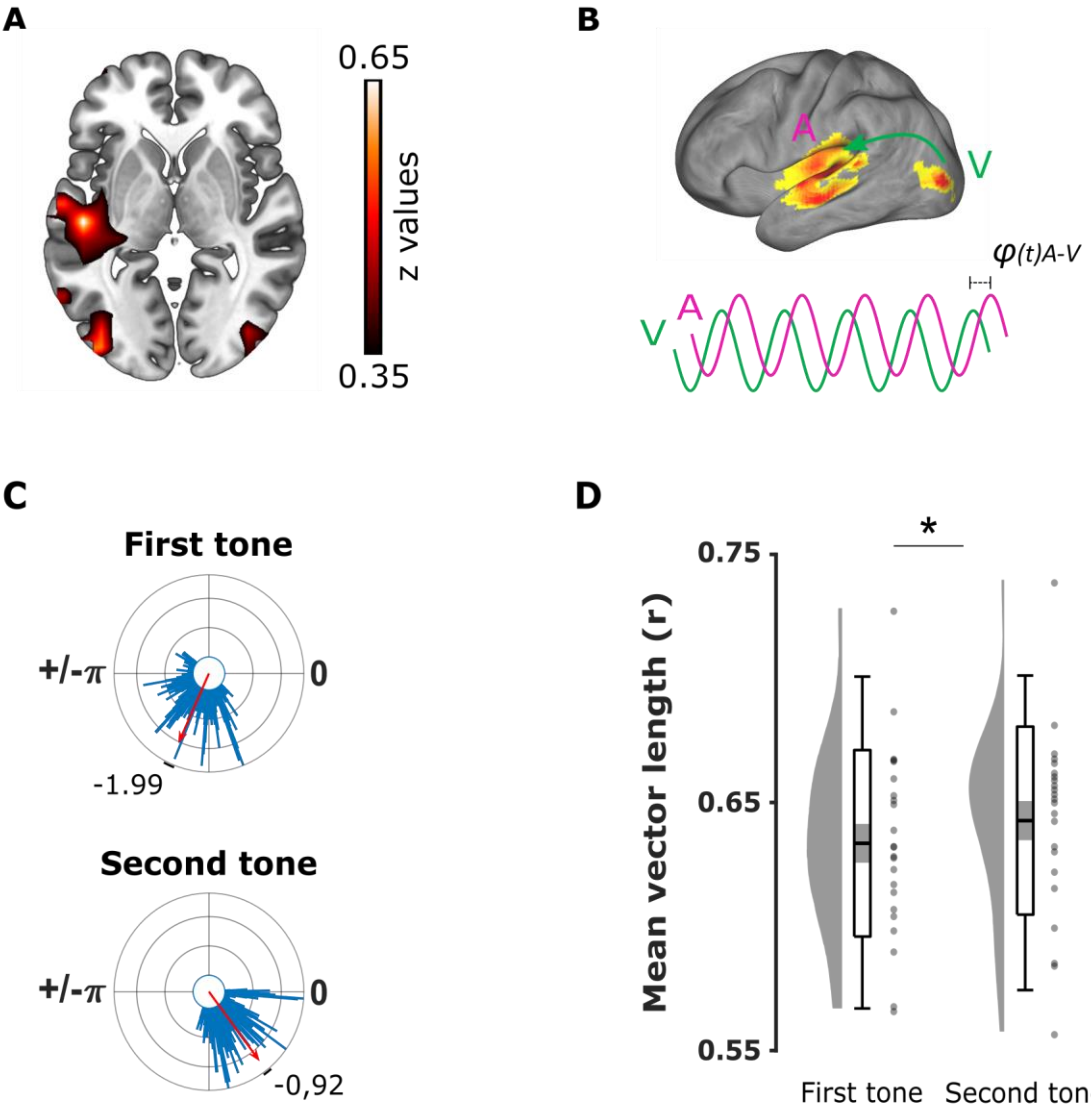

Figure 3: Theta phase coupling analysis between visual and auditory areas during lips perception. (A) Difference of mutual information between the second (2.5 - 5s) and first (0 - 2.5s) time-windows (MI_{second} > MI_{first} contrast; z values). Auditory (MNI coordinates of maximum voxel: [-50 -21 0]; Temporal middle left) and visual (MNI coordinates of maximum voxel: [-40 -89 0]; Occipital middle Left) sources were localized in the left hemisphere. (B) MI_{first} > MI_{second} contrast projected on brain's surface for illustrative purpose: Synchronisation was estimated through ϕ_{A-V} theta phase offset between theta oscillations at identified auditory (pink line) and visual sources (green line) by mean of phase coupling analysis. (C) Audio-visual phase coupling in the first and second time-windows. The mean ϕ_{A-V} offset between auditory and visual theta phases (red arrows) confirmed that oscillations entrained by lip movements in the visual cortex preceded oscillations in the auditory cortex by 1.99 rad (~ 56.10 ms) and 0.92 rad (~ 25.88 ms), respectively in the first and second windows. (D) Theta synchronisation between visual and auditory areas improves with entrainment. The resultant vector length r of the distance between the observed ϕ_{A-V} and the theoretical $\phi_{A-V} = 0$ was greater in the second than the first window, reflecting a more consistent distribution of ϕ_{A-V}. The graphs depict the density, the grand average (mean ± standard error of the mean; errors bars: 95 % confidence interval), and individual resultant vector length r (grey dots). Significance evidenced with a star ($p < 0.05$).

DISCUSSION

In two complementary experiments, we first established that visual entrainment to theta lip phase modulated auditory detection, even if information from silent movies was irrelevant to perform the task. Second, the perception of silent lip movements entrained theta oscillations in the visual cortex, which in turn synchronized with the auditory cortex. Together, these results suggest that the brain's natural reaction to visual speech stimuli might be to align the excitability of the auditory cortex with sharp mouth-openings because that is when one expects to hear corresponding acoustic syllable edges (Hickock & Poeppel, 2007; Giraud & Poeppel, 2012; Peelle & Sommers, 2015 Park et al., 2016; Chandrasekaran et al., 2009). Such a neural process could be a very effective filtering method to increase the sensitivity of the auditory cortex in these relevant time windows for speech comprehension.

Our EEG results suggest that theta oscillations in the left visual cortex encoded the lips' activity first. Then information travelled to the left auditory cortex via phase coupling to shape its activity. Previous findings reported that the auditory cortex tracks both auditory and visual stimulus dynamics using low-frequency neuronal phase modulation during audiovisual movie perception (Luo, Liu and Poeppel, 2010). Other studies reported that the perception of silent lips also recruited the auditory regions (Bourguignon et al., 2020; Cross et al., 2015; Calvert et al., 1997). Our findings go beyond and establish how theta oscillations orchestrate visual and auditory cortices through phase coupling to ensure cross-region communication even in a unimodal condition. Furthermore, it is commonly agreed that entrainment takes several cycles from rhythmic inputs to build up (Doelling et al. 2014; Lakatos et al., 2008; Thut et al., 2011; Zoefel et al. 2018). Behavioural and neural indicators of entrainment reported here consistently increased from the first to the second half time-window of the trial in both experiments. This supports the idea that we indeed observed neural entrainment to lip movements and sheds light on the functional relevance of visual inputs modulating auditory theta rhythms.

As visual onsets naturally lead corresponding auditory onsets by 100-to-300 ms in audiovisual speech (Chandrasekaran et al., 2009; van Wassenhove et al., 2005; Pilling, 2009), visual entrainment to lips may act as a filter by increasing excitability in the auditory cortex to windows containing relevant acoustic features. This hypothesis is corroborated by our phase coupling results where visual theta phase systematically led auditory theta phase during silent movie presentation. However, whether such filtering reflected direct enslavement of the auditory cortex or involved top-down modulations remains unclear. Indeed, higher-level sensorimotor areas also activate during speech perception (Park et al., 2016; 2018; Cognan & Poeppel, 2011; Pulvermüller et al., 2005; Wilson et al., 2004). Assaneo & Poeppel (2018) demonstrated recently that activity in the motor and auditory cortices couple at theta rate during syllable perception, correlating with the strength of coupling between speech signal and EEG in the auditory cortex. On the other hand, motor areas play a role in temporal analysis of rhythmic sensory stimulation (Biau & Kotz, 2018; Arnal et al., 2015; Fujioka et al., 2015; Morillon et al., 2019). Entrainment to lip movements may provide the temporal theta structure of speech signal to motor cortex, which in turn adjusts auditory excitability at critical windows containing the corresponding acoustic

features in a top-down fashion (in line with Park et al. 2015). Alternatively, mouth-opening perception may target internal articulatory representations and help to identify the corresponding sounds in the auditory signal. Theta activity in the auditory cortex would reflect the contribution of endogenous oscillations bearing linguistic inferences generated from motor representations activation. Although speculative, this could partially explain why the increase of entrainment in the auditory cortex was left-lateralized, i.e. by recruiting language-related representations classically associated with the left hemisphere. This hypothesis fits in recent debates on whether neural tracking during speech processing reflects online cooperation between pure entrainment to external salient features and endogenous rhythms providing abstract representations (Meyer, Sun & Martin, 2019; Obleser & Keyser, 2019; Haegens & Zion Golumbic, 2018; Rimmele et al., 2018). However, this would not explain why visual speech information improved the detection of unrelated pure tones here, which will be addressed in future experiments. Additional data-driven analysis suggested that two subpopulations of participants showed distinct visual theta phases shaping auditory perception in the TDT (Figure S2). One could hypothesize that the "good" subpopulation (i.e. group 2) were fine-tuned to a preferred visual theta phase that represents an optimal time-window. This optimal window allowed information to travel to the auditory cortex (either directly or via top-down modulations), and reset auditory activity at "perfect" moments when a tone occurred. Back to our filtering hypothesis, visual theta entrainment would increase auditory excitability coinciding with more time windows containing a tone in this "good" subpopulation regardless of the nature of sounds.

As a final note, although the auditory signal alone often provides enough structural information for the early analytic steps of continuous speech, e.g. telephone conversations, a visual filter may be especially helpful to sharpen auditory perception when hearing is impaired or in elders (Grant et al., 1998). Our results provide an important step toward understanding how visual information functionally drives auditory speech perception, and suggest future directions to investigate hearing loss compensation, i.e. to improve lip-reading along with hearing correction.

AKNOWLEDGMENTS

This work was supported by a sir Henry Wellcome Postdoctoral Fellowship awarded to E.B (Grant reference number: 210924/Z/18/Z), as well as grants from the ERC (Consolidator Grant 647954) and ESRC (ES/R010072/1) awarded to S.H, who is further supported by the Wolfson Foundation and Royal Society. The authors would like to thank people from the Memory and Attention Lab and David Poeppel for their valuable comments and inputs during the preparation of this manuscript.

AUTHOR CONTRIBUTION

E.B, H.P and S.H designed the experiments and paradigms. E.B and D.W collected and analysed the data. E.B, D.W, H.P, O.J and S.H wrote the paper. All the authors discussed the results and commented on the manuscript.

DECLARATION OF INTEREST

The authors of this manuscript declare to have no conflicts of interest.

STAR METHODS

Key resources table:

REAGENT or	SOURCE	IDENTIFIER
Software and Algorithms		
MATLAB	The MathWorks	R2018a
Psychophysics Toolbox	http://psychtoolbox.org	3
FieldTrip	http://www.fieldtriptoolbox.org	v.20161231
SPM8	Wellcome Trust Centre for Neuroimaging	8
ASIO4All	Steinberg Media Technologies	2.12
ActiView	BioSemi B.V. Amsterdam, Netherlands	7
Shotcut	Meltytech, LLC	v.18.06.02
Brainstorm Toolbox	https://neuroimage.usc.edu/brainstorm/	
CARET	Washington University School of Medicine	5.65
Circular Statistics Toolbox	https://uk.mathworks.com/matlabcentral/fileexchange/10676-circular-statistics-toolbox-directional-statistics	v.1.21.0.0
Other		
BioSemi ActiveTwo	BioSemi B.V. Amsterdam, Netherlands	EEG system

system		
ER-3C system	Etymotic Research, Elk Grove Village, IL	EEG compatible earphones
Fastrak	Polhemus, Colchester, VT, USA	Electromagnetic digitiser
ThorLabs DET36A	https://thorlabs.de	Photodetector

Contact for reagent and resource sharing:

Further information and requests for resources and data should be directed to and will be fulfilled by the Lead Contact, Emmanuel Biau (e.biau@bham.ac.uk). Summarized data (cell means) are available; data for individual participants are available, as consent for sharing data at the level of the individual participant was received.

Experimental model and subject details:

Tone detection experiment: Twenty-eight healthy English native speakers (mean age = 19 years ± 0.69; 21 females) took part in the first behavioural experiment. Five participants were left-handed. All of them reported normal or corrected-to-normal vision and hearing. All participants were granted experimental participation credit. The data from four participants were excluded because of extreme overall performances and the final analysis were applied on twenty-four data sets.

Silent movie perception-EEG experiment:

Twenty-five healthy English native speakers (mean age = 21.52 years ± 3.86; 17 females) took part in the first behavioural experiment. All of them reported normal or corrected-to-normal vision and hearing, and were right-handed. Twenty-one participants were granted credits and five participants received financial compensation for their participation (£20). The data from two participants were excluded from the final analyses due to too noisy EEG data. In the two experiments, all the participants signed informed consent and ethical approval was granted by the University of Birmingham Research Ethics Committee, complying with the Declaration of Helsinki.

Method details:

Apparatus:

The two tasks were programmed with Matlab (R2018a; The MathWorks, Natick, MA, USA) and presented with Psychophysics Toolbox (Brainard, 1997; Pelli, 1997; Kleiner et al., 2007). In both tasks, the silent videos were presented on a 21-inch CRT display with a screen refresh rate of 75 Hz (nVidia Quadro K600 graphics card: 875 MHz graphics clock, 1024 MB dedicated graphics memory; Nvidia, Santa Clara, CA, USA). The auditory stimuli in the tone detection task were presented through EEG-compatible insert earphones (ER-3C; Etymotic Research, Elk Grove Village, IL). In the tone detection task, the accuracy of movie and sound presentation timing was optimised by detecting a small white square displayed on the left of the first frame of each visual stimulus with a photodiode (ThorLabs DET36A, thorlabs.de), and Psychophysics Toolbox (PsychPort Audio and ASIO4ALL extensions for Matlab). Additionally, a parallel audio port was used to record the online audio signal of each trial during presentation. Continuous photodiode and audio data during trials were recorded through a BioSemi Analog Input Box (AIB) adding two separate channel inputs into BioSemi ActiveTwo system: the BioSemi AD-box was connected with the AIB through optical fibres. The input from the photodiode was connected through a BNC connector and the input from the microphone was connected through the 3.5 mm audio. Those two inputs were connected to the AIB though a 37 pin Sub-D connector. Data were digitized using the BioSemi ActiView software, with a sampling rate of 2048 Hz. Offline analysis were performed to calculate the real delay between visual and audio stimuli offset using in-house Matlab codes. Any lag between visual and auditory stimuli onsets was later compensated in the data analyses when computing the corresponding visual theta phase to the tones onsets. The experiments were run from a solid-state hard drive on a Windows 7-based PC (3.40 GHz processor, 16 Gb RAM). Participants used a standard computer keyboard to respond to the tasks.

Stimuli of the Tone detection Task:

Movies:

Sixty five-second movies were extracted from natural face-to-face interviews published on YouTube (www.youtube.com) by various universities channels and downloaded via free online application. Satisfying movies containing meaningful content (i.e. one complete sentence, speaker facing toward the camera) were edited using Shotcut (Meltytech, LLC).

For each movie, the video and the sound were exported separately (Video: .mp4 format, 1280 x 720 resolution, 25 frame per second, 200 ms linear ramp fade in/out; Audio: .wav format, 44100 Hz sampling rate, mono).

Lip movements' detection:

Lips contour signal was extracted for each video using in-house Matlab codes. We computed the area information (area contained within the lips contour), the major axis information (horizontal axis within lip contour) and minor axis information (vertical axis within lip contour) as described in Park et al. (2016). In the present study, we used vertical aperture information of the lips contour to establish the theta correspondence between lips and auditory speech (i.e. aperture between the superior and inferior lips) but using area information gave very similar results, as also reported in Park et al. (2016). The lips time-series was resampled at 250 Hz for further analyses with corresponding auditory speech envelope.

Auditory speech signal:

The amplitude envelope of each movie sound was computed using in-house Matlab codes (Park et al., 2018; 2016; Chandrasekaran et al., 2009). First, eight frequency bands equidistant on the cochlear map in the range 100–10,000 Hz were constructed (Smith et al., 2002). Then, sound signals were then band-pass filtered in these bands with a fourth-order Butterworth filter (forward and reverse). Hilbert transform was applied to obtain amplitude envelopes for each band. These signals were then averaged across bands and resulted in a unique wideband amplitude envelope per sound signal. Each final signal was resampled to 250 Hz for further theta correspondence analyses.

Mutual information between lip movements and corresponding auditory speech signal:

To identify the main oscillatory activity conveyed by the lip movements in each visual stimulus, we determined at which theta frequency the auditory and visual speech signals showed significant dependencies. To do so, we examined the audiovisual speech frequency spectrum (1 to 20 Hz) and computed the mutual information (MI) between the minor axis information and speech envelope signals sampled at 250 Hz. MI measures the statistical

dependence between two variables with no prior hypothesis, and with a meaningful effect size measured in bits (Ince et al., 2017; Shannon, 1948). We applied the Gaussian Copula Mutual Information approached described in Ince et al. (2017) in which the MI between two signals corresponds to the negative entropy of their joint copula transformed distribution. This method provides a robust, semiparametric lower bound estimator of MI by combining the statistical theory of copulas together with the closed-form solution for the entropy of Gaussian variables, allowing good estimation over circular variables, like phase as well as power. For each movie, the complex spectrum is normalized by its amplitude to obtain a 2D representation of the phase as points lying on the unit circle for both the lip movements and auditory envelope time-series. The real and imaginary parts of the normalized spectrums are rank-normalized separately and the phase dependence for each frequency between the two 2D signals is estimated using the multivariate GCMI estimator giving a lower bound estimate of the MI between the phases of the two signals. Here, we applied the GCMI analyses in two conditions to determine the frequency of interest in each movie: first, we computed MI between corresponding lips and envelope signals as well as non-matching signals (i.e. lips time-series paired with random auditory envelope signals). For the matching signals, the averaged MI spectrum revealed a greater peak in the expected 4 - 8 Hz theta frequencies, reflected by a bump in the band of interest. In contrast, there was no relationship between random auditory and visual signal pairs, which depicts a flat line profile along the whole spectrum (see Supplementary Information Figure S3 A). These results are well in line with previous studies using coherence or MI measures, and confirm the temporal coupling between lips and auditory speech streams at the expected syllable rate in our videos (Park et al., 2016; 2018; Chandrasekaran et al., 2009). Second, for each movie, we performed a peak detection on the MI spectrum to determine which specific frequency carried most theta information to maximize entrainment in the tone detection and silent movie perception tasks (4Hz frequency peak: 16 videos; 5Hz frequency peak: 15 videos; 6Hz frequency peak: 9 videos; 7Hz frequency peak: 13 videos; 8Hz frequency peak: 7 videos. See Supplementary Information Figure S3 B).

Audio tones and white noise:

Pure auditory tones and white noise stimuli were generated using in-house Matlab codes. The target tone consisted in a sinusoidal signal of 100 ms at one kHz (sampling rate: 44100 Hz). The same noise consisted in a Gaussian white noise lasting two seconds for the calibration task and five seconds in the tone detection task (the white noise has been generated only once and loaded during each procedure to ensure that all the participants were tested with the same noise; sampling rate: 44100 Hz). Both the tone and the white noise signals were normalized between - 1 to 1 (arbitrary units).

Tones onsets:

For each trial, the target tones were embodied in the white noise at predetermined pseudo-random onsets counterbalanced across conditions (zero, one or two tones per trial, 100 trials per condition). In the calibration task serving to determine the individual threshold of target tones detection (see below for the general procedure), there could be only zero or one tone maximum per trial. For the one tone condition, the onset of the target tone always randomly occurred between 300 and 1400 ms after the trial onset to allow participants to detect it properly and have time to respond before the end of the trial. In the zero tone condition, the auditory track consisted in two seconds of white noise only. In the tone detection task, there could be zero, one or two tones per trial. In the one tone condition, the onset of the target always occurred randomly between 300 and 4500 ms after the trial onset. In the two tones condition, the first tone randomly occurred in a time-window centred on the first half of the trial length, between 300 and 3000 ms (mean first tone onsets = 1.68 ± 0.78 s). The second tone occurred in a time-window centred on the second half of the trial length, between 1000 ms after the first tone onset and 4500 ms after the trial onset (mean first tone onsets = 3.45 ± 0.62 s). This design provided participants with enough time to detect and respond to both tones, and kept the two tones temporally unrelated from each other. In the zero tone condition, the auditory track consisted in five-second of white noise only. The signal-to-noise ratio between target tones and white noise was determined for each participant individually with the calibration task performances and adjusted consequently in the following tone detection task (see below).

Procedure of the calibration task and tone detection task (TDT):

The experiment began after the completion of a safety-screening questionnaire and the provision of informed consent. Participants sat in a well-lit testing room at approximatively 60 cm from the centre of the screen and wore the insert earphones for sound presentation. Participants performed first a short pure tone detection task with no visual stimuli (i.e. calibration task). This task served to determine the individual threshold at which each participant detected ~ 70 - 80 % of the target tones in auditory modality only, and the signal-to-noise ratio (SNR) to be implemented between the amplitude of the target tones and the white noise in the following tone detection task (TDT). The calibration task was composed of a four-trial practice to identify the target tone itself, followed by five blocks containing 20 trials each. Each trial began with a black fixation cross (500 - 1000 ms duration, jittered) followed by the presentation of a red cross over a grey background during two seconds to indicate the period of possible target tones occurrence. A continuous white noise was displayed during the red cross presentation. In 50 % of the trials, a unique audio tone was embedded in the white noise at unpredictable onset, and participants had to press "1" key as fast and accurately as possible only when they perceived a target tone. The pseudo-random sequence of the procedure ensured that there were never more than two consecutive trials of the same condition. The participants received no feedback and the procedure continued to the next trial after the end of the two-second white noise. The signal-to-noise ratio was adjusted following an adapted *two-down, one-up* staircase procedure (see Leek, 2001): For the first five trials, the SNR was fixed (mean white noise power of 0.981) and served as a starting point across participants. After each trial, the keypress response of the participant was stored to adjust the SNR for the next trial as following: for two successive hits, the SNR was decreased by 2 % of the starting signal energy in the next trial. For two successive correct rejections (i.e. no response when no tone occurred) or one correct rejection following a hit, the SNR was kept identical for the next trial. After a miss or a false alarm, the SNR was always increased by 2 % of the starting signal energy. At the end of the calibration task, the individual SNR was averaged over the last 30 trials and stored for the following real tone detection task (mean calibration accuracy rate: 0.75 ± 0.05). The participants took a short break and were recalled the instructions before starting the proper tone detection task. The calibration task lasted approximatively seven minutes.

The main structure of the TDT was the same as in the precedent calibration task. The TDT was composed of a short four-trial practiced followed by 300 trials divided in 6 blocks of 50 trials each and separated by breaks (the sixty silent movies were repeated five times each to generate the total 300 trials). Each trial began with a red fixation cross presentation (500-1250 ms duration, jittered). Then, a random five-second silent movie was presented with a black fixation cross in the centre of the screen to give the participants a point to gaze at and reduce saccades. The continuous white noise was displayed together with the silent movie according to the three random conditions: no tone (100 trials), one single tone (100 trials) or two tones (100 trials) hidden in the white noise. Participants were instructed to press "1" key as fast and accurately as possible only when they perceived a target tone. The participants received no feedback on their responses and the procedure continued with the next trial after the end of the silent movie. The SNR between the tones and the white noise was determined in the previous calibration task as explained above. The TDT lasted approximatively 50 minutes.

TDT conditions:

The condition of interest containing the two tones (i.e. first and second tone) served to assess our main hypothesis that entrainment increases in time with the perception of visual information conveyed by the speakers' lip movements. According to this, the second tones should be better detected and associated to a greater theta entrainment as compared to the first tones to reflect enslavement of the auditory system by the entrained visual system to lip movements. The zero and single tone conditions were additional control conditions: the zero tone condition served to determine the false alarm rates (i.e. participants' keypresses in the absence of tone) and controlled whether participants tended to press more together with the tone onset delays (i.e. time-dependent response bias). The single tone condition served to counterbalance the number of trials containing two tones and control for the predictability of the second tone. The replication of the performances observed in the two tones condition by sorting the single tones according to their onsets equivalent to either first or second tone onsets would confirm that the detection of the second tone is not due to its predictability from a preceding tone but its position in time

only. The pseudo-random sequence of the procedure ensured that there were never more than three consecutive trials of the same condition.

Perception of silent movies-EEG task:

Movies:

The movies presented during the silent lips perception task were the exact same 60 movies used in the previous tone detection task. The order of movies was randomized across participants.

Procedure:

Participants sat in a well-lit testing room at approximatively 60 cm from the centre of the screen to complete a safety-screening questionnaire and the provision of informed consent first. After the correct preparation of the EEG cap, the participants were instructed to attend to all the movies quietly and to avoid movements during the presentation. Each trial was preceded by a central fixation cross (500 - 1250 ms duration, jittered) followed by the presentation of a random five-second movie. A central fixation cross was displayed during the movie presentation to give participants a point to gaze at and reduce excessive saccades. Participants were instructed to attend to each movie carefully and rate its emotional content based on speaker's facial gestures by using the number keys on the keyboard after the presentation (i.e. 1 for neutral through 5 for very emotional; results not reported). The total presentation of the sixty movies lasted approximatively 10 minutes.

Online EEG recordings: Continuous EEG signal was recorded using a 128 channel BioSemi ActiveTwo system (BioSemi, Amsterdam, Netherlands). Vertical and horizontal eye movements were recorded from additional electrodes placed approximatively one cm to the left of the left eye, one cm to the right of the right eye, and one cm below the left eye. Online EEG signals were digitalized using BioSemi ActiView software at a sampling rate of 2048 Hz. For each participant, the position of the electrodes on the scalp were tracked using a Polhemus FASTRAK device (Colchester) and recorded with Brainstorm (Tadel et al., 2011) implemented in MATLAB.

Offline EEG preprocessing: EEG data were preprocessed offline using Fieldtrip (Oostenveld et al., 2011) and SPM8 toolboxes (Wellcome Trust Centre for Neuroimaging). Continuous EEG signals were bandpass filtered between one and 100 Hz and bandstop filtered (48–52 Hz and 98–102 Hz) to remove line noise at 50 and 100 Hz. Data were epoched from 2000 ms before stimulus onset to 7000 ms after stimulus onset, and downsampled to 512 Hz. Bad trials and channels with artefacts were excluded by visual inspection and numerical criteria (e.g., variance as well as kurtosis) before applying an independent component analysis (ICA) to remove components related to ocular artefacts. Bad channels were then interpolated using the method of triangulation of nearest. After re-referencing the data to average reference, trials with artefacts were manually rejected by a last visual inspection. On average, 4.48 ± 2.48 trials were removed and 4.04 ± 1.82 channels were interpolated per participants.

Head models:

For the 22 participants without individual MRI scans, the MNI-MRI and the volume conduction templates provided by Fieldtrip were used to construct the head models. Electrode positions of each participant were aligned to the template head model. Source models were prepared with the template volume conduction model and the aligned individuals' electrode positions following standard procedures. One participant provided his own MRI scans and his head model was built using his structural scans (Michelmann et al., 2016): the MRI scans were segmented into four layers (i.e. brain, CSF, skull and scalp) using the Statistical Parametric Mapping 8 (SPM8; http://www.fil.ion.ucl.ac.uk/spm) and Huang toolboxes (Huang et al., 2013). The volume conduction model was constructed using the dipoli method implemented in Fieldtrip. Participant's electrode positions were aligned to his individual head model. Finally, his MRI was warped into the same MNI template MRI of Fieldtrip and the inverse of the warp was applied to a template dipole grid to have each grid point position in the same normalized MNI space as the other participants for further group analyses.

Source localization during silent movie perception:

552 Source analyses on EEG data recorded during silent movies presentation were run using
553 individual electrode positions, grid positions and template volume conduction model. For
554 the participant who had his MRI scans, source analyses were calculated using normalized
555 grid positions instead. Source activity was reconstructed using a linearly constrained
556 minimum variance beamforming method implemented in Fieldtrip (LCMV; see Van Veen et
557 al., 1997). The neural entrainment to lip movements at source level was determined by
558 computing mutual information between EEG epochs and the lip movements during silent
559 movie presentation (i.e. lips time-series from the silent movie presented during the trial). To
560 test our hypothesis that entrainment builds up in time with perceived theta lips activity, we
561 contrasted the difference of MI between the equivalent time-window to the second tone
562 window (MI_{second}), and the equivalent time-window to the first tone window (MI_{first}) in the
563 previous TDT. Accordingly, we expected first to observe an increase of theta activity in the
564 visual cortex reflecting entrainment to lip movements. Second, we expected an equivalent
565 pattern in the auditory correlates reflecting a tuning from visual activity. For each single
566 trial, MI was first computed separately in the equivalent first (0 to 2.5 seconds after trial
567 onset; MI_{first}) and second time-windows (2.5 to 5 seconds after trial onset; MI_{second}) at the
568 2020 virtual electrodes by using the same approach described in the stimuli analysis section
569 (i.e. where we established which frequency carried most correspondence between lips and
570 envelope signals for each video; using a wavelet transform to compute the phase). Second,
571 for each single trial, the MI spectrum was realigned respect to the frequency bin (± 2 Hz)
572 corresponding to the peak of MI between lips and envelope signal established in the movie
573 analyses. This step was done to be able to average all the trials together taking into account
574 the main theta activity carried in each individual movie. For instance, if the peak of MI
575 between lip movements and auditory envelope was found at 4 Hz in the video number 1,
576 the realigned MI spectrum between EEG and lips signals from the trials presenting video
577 number 1 was now 4 ± 2 Hz (2 to 6 Hz; 1 Hz bin) to insure that the central bin of each single
578 trial corresponds to the objectively determined frequency peak of theta activity. Third, the
579 realigned MIs of single trials were averaged across trials within each participant for further
580 group analyses. For each participant, we calculated the normalized difference of MI at the
581 frequency bin of interest (MI normalization: $(MI_{second} - MI_{first})/ MI_{first}$; third bin in the
582 realigned MI spectrum) in the equivalent second tone window minus equivalent first tone

583 window at all the 2020 virtual electrodes. Finally, the normalized difference of MI between
584 second and first tone time-windows was grand averaged across participants and the grand
585 average was interpolated to the MNI MRI template. The coordinates for auditory and visual
586 sources of interest were determined by finding the maximum of MI_{second} - MI_{first} differences
587 in regions corresponding to the auditory and visual areas, and defined using the automated
588 anatomical labelling atlas (AAL).

589 Source reconstruction:

590 We performed time-series reconstruction analysis to investigate the synchronization at
591 theta activity between the two sources of interest during silent movie presentation. The
592 time series data were reconstructed and extracted at the visual and auditory coordinates
593 determined by source localization analysis. LCMV beamformer reconstruction can cause
594 random direction of source dipoles and eventually affect phase analysis results. To get
595 around this issue, the event-related potentials (ERP) time-locked to movie onsets at visual
596 and auditory sources were plotted to identify the visual component, i.e. N1-P2-N2
597 waveform (Wang et al., 2018). After visual inspection, the sign of the reconstructed data
598 were flipped in direction by multiplying the time-series by -1 if any visual or auditory source
599 ERPs showed the opposite of the expected direction of a visual component (i.e. negative-
600 positive-negative polarity). This "flipping" correction was applied consistently across all trials
601 before sorting data between first and second time-windows, thus it did not bias results
602 towards our hypothesis. The same phase coupling analyses were computed with unflipped
603 source data as a control. Phase angle differences between visual and auditory theta
604 activities in the first and second windows were also non-uniformly distributed according to
605 Rayleigh tests with significantly different mean angles according to a Kuiper's test,
606 confirming that the flipping procedure only better reflected phase coupling modulation with
607 entrainment.

608 Theta phase coupling between auditory and visual sources:

609 First, auditory signal was projected orthogonally onto the visual signal applying a Gram-
610 Schmidt process (GSP; Hipp et al., 2012) for single trials before computing phase
611 information. This was done to reduce the noise correlation patterns reflecting activity from

a common source (i.e. volume conduction) estimate captured at different electrodes (in that case, the phase alignment reflects the same source activity and not the phase coupling between two distinct source activities). The GSP increases the signal-to-noise ratio by leaving intact the proper activities conveyed at the two distinct electrodes while reducing noise correlation weight (see Hipp et al., 2012). Second, for each trial the instantaneous theta phase of the auditory and visual orthogonalized time-series were computed by applying a Hilbert transform with a bandpass filter centred on the frequency bin of MI peak ± 2 Hz, accordingly to the mean theta frequency of the video presented during the trial. Third, the difference of unwrapped instantaneous phase between auditory and visual sources was computed for each single trial at each time-point in two windows corresponding to the first (0.5 to 2 seconds after trial onset) and second tone windows (3 to 4.5 seconds after trial onset). The first and last 500 ms at the edges of the epoch were not included into phase coupling analyses to avoid the trial onset and offset responses. Additionally, the phase-slope index (PSI) was calculated in the first and second time-windows between the left auditory and visual sources to estimate the directionality of information flow between our two sources of interest, using Fieltrip procedure (Nolte et al., 2008). PSI analysis revealed negative values in both time-windows (respectively $psi_{first\ tone}$ = -0.035 ± 0.055 and $psi_{second\ tone}$ = -0.041 ± 0.035), confirming that that the left visual source led the left auditory source during silent movie perception.

Quantification and statistical analysis:

The Tone Detection and the Silent lips perception tasks were within-subject design.

Tone detection performance:

Tone detection performances: The hits (i.e. correctly detected tones) and false alarms (i.e. keypress responses during the zero tone condition allocated to the first or second tone window depending on their onsets) rates were computed to calculate the individual mean sensitivity index (i.e. d') in the two conditions for each participant (i.e. single tone and two tones conditions). The reaction times of the hits were computed to calculate the individual mean reaction times in the two conditions for each participant (i.e. single tone and two tones conditions). Additionally, we calculated the mean correct response rates and reaction

times of the two conditions concatenated together of each individual to exclude blindly potential outliers without favouring the results towards our hypothesis and performing as following: below chance level (correct response rate < 0.5) or perfectly (correct response rate = 1), or with mean reaction times outside the grand averaged reaction times ± two standard deviations range. Accordingly, four participants were excluded from analyses (two participants performed below chance level, one participant performed perfectly and one participant's reaction times were slower than the grand average mean + two standard deviations). A paired-samples t-test was conducted on the averaged d' scores and hit reaction times between the first and second tones in the two tones condition and single tone condition separately. Additionally, a paired-samples t-test was performed on false alarm rates from the first and second windows in the zero tone condition to control for any response bias with time.

Visual entrainment to theta activity conveyed by lip movements:

To bridge visual entrainment to auditory processing together, we related the tone target onsets to the theta activity conveyed by the lip movements during silent movies perception: First, for each movie the theta phase of the lip movements' time-series was computed by applying a Hilbert transform with a bandpass filter centred on the frequency bin of MI peak ± 2 Hz, accordingly to the mean theta frequency determined in MI stimuli analyses. Second, we computed the instantaneous theta phase of the lips signal corresponding to the onset of the tones occurring during each trial. All further circular statistics on angular scale were performed using the CircStat toolbox on Matlab (Berens, 2009). The circular uniformity in the first and second tones windows within and across participants were estimated separately by applying Rayleigh tests to calculate the mean direction and resultant vector length from hits/miss trials. To assess statistically the strength of visual entrainment between the first and second tone windows in the two tones condition (hits only), we performed a permutation test on the resultant vector length difference (z-value) second tone minus first tone reflecting the effect size. For each participant, we generated 10000 iterations as following: first, the hit trial labels were shuffled between the first and second tones in the two tones condition. Second, two balanced subsamples of shuffled trials were selected, with a number matching the smallest number of trials between the first and

second tone hits. Third, the mean phase of the first and second tone shuffled trials were computed for each iteration and per participant. Fourth, a Rayleigh's test of uniformity was applied on the mean phases to determine a resultant vector length at the first and second tones per iteration (i.e. z-value). For each iteration, we computed the difference of z-value$_{\text{second tone}}$ - z-value$_{\text{first tone}}$ to quantify its effect size, and the resultant 10000 z-value differences were sorted in descending order. To estimate the final p-value and test the null hypothesis, the difference of z-value between the original first and second tone data was ranked in the sorted permuted z-value differences and divided by the total number of permutations+1. If the p-value was smaller than $\alpha = 0.05$, we rejected the null hypothesis H_0 = there is no difference of resultant vector length between the first and second tones (i.e. the visual entrainment is significantly greater in the second tone window). The exact same approach was applied on the single tone condition, as well as on the hit versus miss entrainment comparisons.

Subpopulations of group 1 and group 2:

Participants were sorted in two subpopulations according to their preferred theta phase in the second tone window, were visual entrainment supposedly took place after enough lip movements inputs in the condition of interest (i.e. two tones condition). The Rayleigh tests revealed non-uniform distributions of preferred phase at the second tones for group 1 ($n = 11$; $\mu = 348.83°$; $p < 0.001$) and group 2 ($n = 10$; $\mu = 249.63°$; $p < 0.001$). A Kuiper two-sample test confirmed that the mean preferred phases were different between group 1 and 2 ($k = 121$; $p < 0.01$).

Audio-visual theta synchrony in the silent lips perception-EEG task:

The phase coupling between auditory and visual sources was estimated through their theta phase angle difference in time-windows equivalent to the first and second tone windows from the TDT. To quantify the improvement of phase coupling with entrainment, we computed the resultant vector length r of the distance between the observed $\phi_{A\text{-}V}$ in the data and a fixed $\phi_{A\text{-}V} = 0$ in the first and second windows separately ($\phi_{A\text{-}V} = 0$ meaning that visual and auditory theta phases are perfectly aligned with a constant offset of zero at each time-point of the time-window). A better synchrony between visual and auditory areas

would be reflected by a more consistent distribution of $\phi_{A\text{-}V}$ towards a particular angle (i.e. 0). For each trial, we calculated the resultant vector length of the distance between the real auditory-visual phase offset and the theoretical phase offset 0° at each time point in the two time-windows. The resultant vector length was collapsed across time in the first and second windows separately, resulting in two values per trial. Single-trial values in the first and second windows were then averaged across trials for each participant, and the difference of phase entrainment values was assessed with a paired samples t-test.

SUPPLEMENTARY INFORMATION

Supplemental Information includes four figures, one silent movie (Video_1) and one white noise containing two tones (Audio_1) used in the TDT and EEG tasks.

REFERENCES

Chandrasekaran, C., Trubanova, A., Stillittano, S., Caplier, A., & Ghazanfar, A. A. (2009). The natural statistics of audiovisual speech. *PLoS Computational Biology*, *5*(7), e1000436. https://doi.org/10.1371/journal.pcbi.1000436

Giraud, A.-L., & Poeppel, D. (2012). Cortical oscillations and speech processing: emerging computational principles and operations. *Nature Neuroscience*, *15*(4), 511–517. https://doi.org/10.1038/nn.3063

Park, H., Ince, R. A. A., Schyns, P. G., Thut, G., & Gross, J. (2015). Frontal Top-Down Signals Increase Coupling of Auditory Low-Frequency Oscillations to Continuous Speech in Human Listeners. *Current Biology*, *25*(12), 1649–1653. https://doi.org/10.1016/j.cub.2015.04.049

Bourguignon, M., Baart, M., Kapnoula, E. C., & Molinaro, N. (2020). Lip-reading enables the brain to synthesize auditory features of unknown silent speech. *Journal of Neuroscience*, *40*(5), 1053–1065. https://doi.org/10.1523/jneurosci.1101-19.2019

Crosse, M. J., Butler, J. S., & Lalor, E. C. (2019). Congruent Visual Speech Enhances Cortical Entrainment to Continuous Auditory Speech in Noise-Free Conditions. *The Journal of*

Neuroscience : The Official Journal of the Society for Neuroscience, *35*(42), 14195–14204. https://doi.org/10.1523/jneurosci.1829-15.2015

Calvert, G. A., Bullmore, E. T., Brammer, M. J., Campbell, R., Williams, S. C. R., McGuire, P. K., Woodruff, P.W., Iversen, S.D., & David, A. S. (1997). Activation of auditory cortex during silent lipreading. *Science*, *276*(5312), 593–596. https://doi.org/10.1126/science.276.5312.593

Park, H., Kayser, C., Thut, G., & Gross, J. (2016). Lip movements entrain the observers' low-frequency brain oscillations to facilitate speech intelligibility. *ELife*, *5*. https://doi.org/10.7554/eLife.14521

Luo, H., & Poeppel, D. (2007). Phase patterns of neuronal responses reliably discriminate speech in human auditory cortex. *Neuron*, *54*(6), 1001–1010. https://doi.org/10.1016/j.neuron.2007.06.004

Keitel, A., Gross, J., & Kayser, C. (2018). Perceptually relevant speech tracking in auditory and motor cortex reflects distinct linguistic features. *PLoS Biology*, *16*(3), e2004473. https://doi.org/10.1371/journal.pbio.2004473

Peelle, J. E., & Davis, M. H. (2012). Neural Oscillations Carry Speech Rhythm through to Comprehension. *Frontiers in Psychology*, *3*, 320. https://doi.org/10.3389/fpsyg.2012.00320

Gross, J., Hoogenboom, N., Thut, G., Schyns, P., Panzeri, S., Belin, P., & Garrod, S. (2013). Speech Rhythms and Multiplexed Oscillatory Sensory Coding in the Human Brain. *PLoS Biology*, *11*(12), e1001752. https://doi.org/10.1371/journal.pbio.1001752

Meyer, L., Sun, Y., & Martin, A. E. (2019). Synchronous, but not entrained: exogenous and endogenous cortical rhythms of speech and language processing. *Language, Cognition and Neuroscience*, 1–11. https://doi.org/10.1080/23273798.2019.1693050

750 Obleser, J., & Kayser, C. (2019). Neural Entrainment and Attentional Selection in the
751 Listening Brain. *Trends in Cognitive Sciences*, Vol. 23, pp. 913–926.
752 https://doi.org/10.1016/j.tics.2019.08.004

753 Haegens S, Zion Golumbic E. (2018). Rhythmic facilitation of sensory processing: A critical
754 review. *Neurosci Biobehav Rev*, *86*:150-165. doi:10.1016/j.neubiorev.2017.12.002

755 Rimmele, J. M., Morillon, B., Poeppel, D., & Arnal, L. H. (2018). Proactive Sensing of Periodic and
756 Aperiodic Auditory Patterns. *Trends in Cognitive Sciences*, 22, 870–882.
757 https://doi.org/10.1016/j.tics.2018.08.003

758 Park, H., Ince, R. A. A., Schyns, P. G., Thut, G., & Gross, J. (2018). Representational
759 interactions during audiovisual speech entrainment: Redundancy in left posterior
760 superior temporal gyrus and synergy in left motor cortex. *PLoS Biology*, *16*(8).

761 Crosse, M.J, ElShafei, H.A, Foxe, J.J, and Lalor E.C. (2015). Investigating the Temporal
762 Dynamics of Auditory Cortical Activation to Silent Lipreading. 7th Annual International
763 IEEE EMBS Conference on Neural Engineering

764 Hanslmayr, S., Axmacher, N., & Inman, C. S. (2019, July 1). Modulating Human Memory via
765 Entrainment of Brain Oscillations. *Trends in Neurosciences*, Vol. 42, pp. 485–499.
766 https://doi.org/10.1016/j.tins.2019.04.004

767 Thut, G., Veniero, D., Romei, V., Miniussi, C., Schyns, P., & Gross, J. (2011). Rhythmic TMS
768 causes local entrainment of natural oscillatory signatures. *Current Biology*, *21*(14),
769 1176–1185. https://doi.org/10.1016/j.cub.2011.05.049

770 Hickok, G., & Poeppel, D. (2007, May). The cortical organization of speech processing.
771 *Nature Reviews Neuroscience*, Vol. 8, pp. 393–402. https://doi.org/10.1038/nrn2113

772 Peelle, J. E., & Sommers, M. S. (2015). Prediction and constraint in audiovisual speech
773 perception. *Cortex; a Journal Devoted to the Study of the Nervous System and Behavior*,
774 *68*, 169–181. https://doi.org/10.1016/j.cortex.2015.03.006

775 Luo, H., Liu, Z., & Poeppel, D. (2010). Auditory cortex tracks both auditory and visual
776 stimulus dynamics using low-frequency neuronal phase modulation. *PLoS Biology*, *8*(8),
777 25–26. https://doi.org/10.1371/journal.pbio.1000445

778 Doelling, K. B., Arnal, L. H., Ghitza, O., & Poeppel, D. (2014). Acoustic landmarks drive delta-
779 theta oscillations to enable speech comprehension by facilitating perceptual parsing.
780 *NeuroImage*, *85 Pt 2*, 761–768. https://doi.org/10.1016/j.neuroimage.2013.06.035

781 Lakatos, P., Karmos, G., Mehta, A. D., Ulbert, I., & Schroeder, C. E. (2008). Entrainment of
782 neuronal oscillations as a mechanism of attentional selection. *Science (New York, N.Y.)*,
783 *320*(5872), 110–113. https://doi.org/10.1126/science.1154735

784 Zoefel, B., Archer-Boyd, A., & Davis, M. H. (2018). Phase Entrainment of Brain Oscillations
785 Causally Modulates Neural Responses to Intelligible Speech. *Current Biology*, *28*(3),
786 401-408.e5. https://doi.org/10.1016/j.cub.2017.11.071

787 van Wassenhove, V., Grant, K. W., & Poeppel, D. (2005). Visual speech speeds up the neural
788 processing of auditory speech. *Proceedings of the National Academy of Sciences of the*
789 *United States of America*, *102*(4), 1181–1186.
790 https://doi.org/10.1073/pnas.0408949102

791 Pilling, M. (2009). Auditory event-related potentials (ERPs) in audiovisual speech perception.
792 *Journal of Speech, Language, and Hearing Research : JSLHR*, *52*(4), 1073–1081.
793 https://doi.org/10.1044/1092-4388 (2009/07-0276)

794 Cogan, G. B., & Poeppel, D. (2011). A mutual information analysis of neural coding of speech
795 by low-frequency MEG phase information. *Journal of Neurophysiology*, *106*(2), 554–
796 563. https://doi.org/10.1152/jn.00075.2011

797 Pulvermüller, F., Huss, M., Kherif, F., Del Prado Martin, F. M., Hauk, O., & Shtyrov, Y. (2006).
798 Motor cortex maps articulatory features of speech sounds. *Proceedings of the National*
799 *Academy of Sciences of the United States of America*, *103*(20), 7865–7870.
800 https://doi.org/10.1073/pnas.0509989103

801 Wilson, S. M., Saygin, A. P., Sereno, M. I., & Iacoboni, M. (2004). Listening to speech
802 activates motor areas involved in speech production. *Nature Neuroscience*, *7*(7), 701–
803 702. https://doi.org/10.1038/nn1263

804 Assaneo, F., M., & Poeppel, D. (2018). The coupling between auditory and motor cortices is
805 rate-restricted: Evidence for an intrinsic speech-motor rhythm. Sci Adv, 4(2). DOI:
806 10.1126/sciadv.aao3842

807 Biau, E., & Kotz, S. A. (2018). Lower beta: A central coordinator of temporal prediction in
808 multimodal speech. *Frontiers in Human Neuroscience*, Vol. 12.
809 https://doi.org/10.3389/fnhum.2018.00434

810 Arnal, L. H., Doelling, K. B., & Poeppel, D. (2015). Delta-Beta Coupled Oscillations Underlie
811 Temporal Prediction Accuracy. *Cerebral Cortex*, *25*(9), 3077–3085.
812 https://doi.org/10.1093/cercor/bhu103

813 Fujioka, T., Ross, B., & Trainor, L. J. (2015). Beta-Band Oscillations Represent Auditory Beat
814 and Its Metrical Hierarchy in Perception and Imagery. *Journal of Neuroscience*, *35*(45),
815 15187–15198. https://doi.org/10.1523/jneurosci.2397-15.2015

816 Morillon, B., Arnal, L. H., Schroeder, C. E., & Keitel, A. (2019, December 1). Prominence of
817 delta oscillatory rhythms in the motor cortex and their relevance for auditory and
818 speech perception. *Neuroscience and Biobehavioral Reviews*, Vol. 107, pp. 136–142.
819 https://doi.org/10.1016/j.neubiorev.2019.09.012

820 Grant, K. W., Walden, B. E., & Seitz, P. F. (1998). Auditory-visual speech recognition by
821 hearing-impaired subjects: consonant recognition, sentence recognition, and auditory-
822 visual integration. *The Journal of the Acoustical Society of America*, *103*(5 Pt 1), 2677–
823 2690. https://doi.org/10.1121/1.422788

824 Brainard, D.H. (1997). The psychophysics toolbox. *Spat. Vis. 10*, 433–436

825 Pelli, D.G. (1997). The VideoToolbox software for visual psychophysics: transforming
826 numbers into movies. *Spat. Vis. 10*, 437–442

827 Kleiner, M., Brainard, D., Pelli, D., Ingling, A., Murray, R., and Broussard, C (2007). What's
828 new in psychtoolbox-3. *Perception, 36*, 1–16

829 Smith, Z. M., Delgutte, B., & Oxenham, A. J. (2002). Chimaeric sounds reveal dichotomies in
830 auditory perception. *Nature*, *416*(6876), 87–90. https://doi.org/10.1038/416087a

831 Ince, R. A. A., Giordano, B. L., Kayser, C., Rousselet, G. A., Gross, J., & Schyns, P. G. (2017). A
832 statistical framework for neuroimaging data analysis based on mutual information
833 estimated via a gaussian copula. *Human Brain Mapping*, *38*(3), 1541–1573.
834 https://doi.org/10.1002/hbm.23471

835 Shannon C. E. (1948). The mathematical theory of communication. *Bell Syst Tech J*, 27:379

836 Leek, M. R. (2001). Adaptive procedures in psychophysical research. *Perception and*
837 *Psychophysics*, *63*(8), 1279–1292. https://doi.org/10.3758/BF03194543

838 Tadel F, Baillet S, Mosher JC, Pantazis D, Leahy RM (2011) Brainstorm: a user-friendly
839 application for MEG/EEG analysis. *Comput Intell Neurosci, 2011*:879716

840 Oostenveld R, Fries P, Maris E, Schoffelen JM (2011) FieldTrip: open source software for
841 advanced analysis of MEG, EEG, and invasive electrophysiological data. *Comput Intell*
842 *Neurosci, 2011*:156869

843 Michelmann S, Bowman H, Hanslmayr S (2016) The temporal signature of memories:
844 identification of a general mechanism for dynamic memory replay in humans. *PLOS*
845 *Biol, 14*:e1002528

846 Huang Y, Dmochowski JP, Su Y, Datta A, Rorden C, Parra LC (2013) Automated MRI
847 segmentation for individualized modeling of current flow in the human head. *J Neural*
848 *Eng, 10*:066004

849 Van Veen BD, van Drongelen W, Yuchtman M, Suzuki A (1997) Localization of brain electrical
850 activity via linearly constrained minimum variance spatial filtering. *IEEE Trans Biomed*
851 *Eng, 44*:867– 880

852 Wang, D., Clouter, A., Chen, Q., Shapiro, K. L., & Hanslmayr, S. (2018). Single-Trial Phase
853 Entrainment of Theta Oscillations in Sensory Regions Predicts Human Associative
854 Memory Performance. *The Journal of Neuroscience : The Official Journal of the Society*
855 *for Neuroscience*, *38*(28), 6299–6309. https://doi.org/10.1523/JNEUROSCI.0349-
856 18.2018

857 Hipp, J. F., Hawellek, D. J., Corbetta, M., Siegel, M., & Engel, A. K. (2012). Large-scale cortical
858 correlation structure of spontaneous oscillatory activity. *Nature Neuroscience*, *15*(6),
859 884–890. https://doi.org/10.1038/nn.3101

860 Berens, P. (2009). CircStat: A MATLAB Toolbox for Circular Statistics. *Journal of Statistical*
861 *Software, 31*(10), 1 - 21. doi:http://dx.doi.org/10.18637/jss.v031.i10.

862 **SUPPLEMENTARY INFORMATION**

863

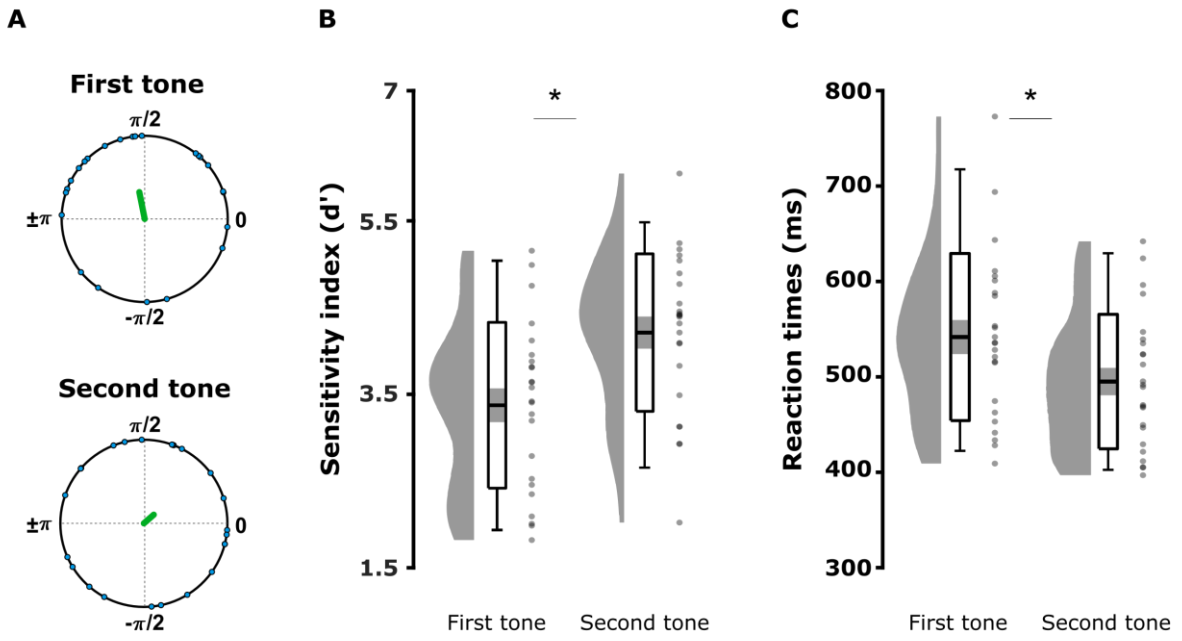

864

865 **Figure S1: Visual entrainment and tone detection performance in the single tone**
866 **condition.** Each single tone was sorted as a first or second tone according to its onset, i.e.
867 between 0 and 2.5 s or 2.5 and 5s after trial onset. (A) Resultant r vector length (green line)
868 from grand average phase at the onsets of first tones hits (n = 24; μ = 1.769 rad or 101.336°;
869 r_{first} = 0.329; p = 0.074) and second tones hits (n = 24; μ = 0.719 rad or 41.165°; r_{second} =

0.157; p = 0.558). The individual mean theta phases are depicted in polar coordinates (blue circles). (B) Mean sensitivity index (d') and (C) reaction times. The graphs depict the density, the grand average (mean ± standard error of the mean; errors bars: 95 % confidence interval), and individual means (grey dots) for tones sorted as first or second ones. Significant contrasts are evidenced with stars. A permutation test on the resultant vector length difference between the tones sorted as first and second tones did not reveal significant difference (figure S1 A; permutations: 10000; effect size = - 0.172; p = 0.835). Two paired-samples t-test performed on d' scores and reaction times confirmed that the second tones were better detected (figure S1 B; T(1, 23) = -4.114; p < 0.001; two-tailed), and faster as compared to the first tones (figure S1 C; T(1, 23) = 4.778; p < 0.001; two-tailed). Finally, we compared the tone detection performances between the single tone and two tones conditions by mean of 2-by-2 repeated-measures ANOVAs (factors condition and tone position). A main effect of position showed that the second tones were better detected than the first tones in both conditions (F(1, 23) = 19.174; p < 0.001). No main effect of condition (F(1, 23) = 1.017; p = 0.324) or interaction between condition and tone position on d' were found (F(1, 23) = 0.567; p = 0.459). A repeated-measures ANOVA on reaction times showed a significant effect of tone position with faster responses to second tones than first tones (F(1, 23) = 33.797; p < 0.001). Additionally, a significant effect of condition showed overall faster reaction times in the two tones condition as compared to the single tone condition (F(1, 23) = 14.047; p = 0.001), but no interaction between tone position and condition (F(1, 23) = 0.173; p = 0.682).

Distinct preferred phases showed performance differences between two subpopulations of listeners.

The behavioural data of the TDT task suggests that two separate subpopulations entrained to different preferred theta phases in the second tone time-window (see Figure 2A lower panel and Figure S2B below). In a post-hoc analysis, we assessed whether these apparently distinct populations also showed differences in tone detection performances. Arguably, any difference should be most pronounced only when visual entrainment eventually took place (second tone window) but not early in the trial. Participants were

sorted in two groups based on their mean theta phase in the second tone window (i.e. n_{group1} = 11 and n_{group2} = 10; see STAR Methods) and we compared detection performance (d') in the two tones condition by means of a repeated-measures ANOVA (with factors tone position and group).

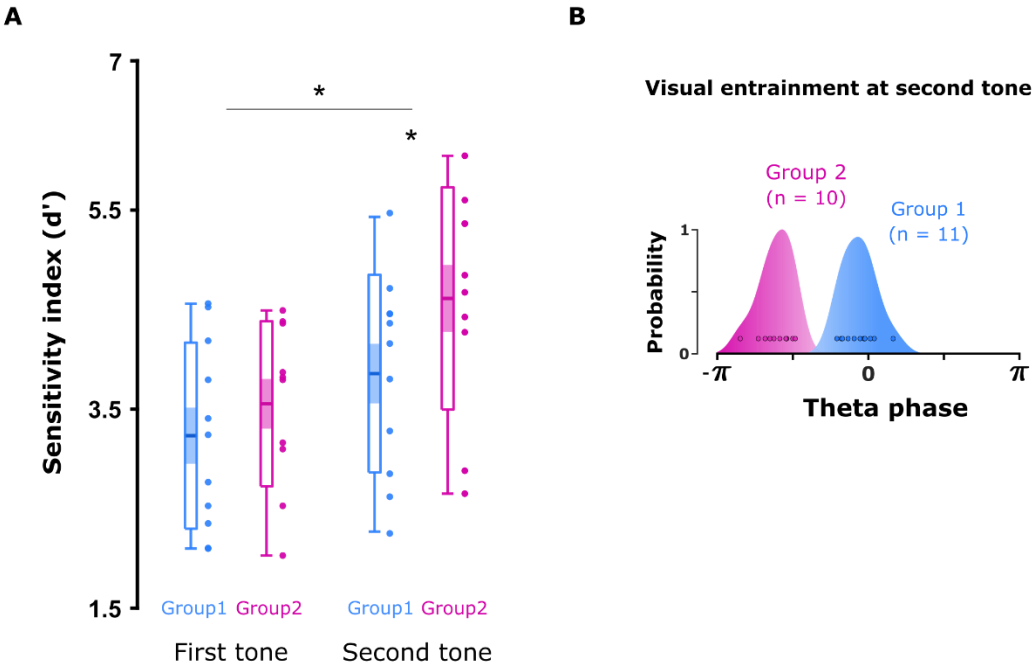

Figure S2: Preferred theta phase predicted tone detection task performance. (A) Tone detection sensitivity (d') of first and second tones between the group 1 and 2. The graphs depict the density, the grand average (mean ± standard error of the mean; errors bars: 95 % confidence interval), and individual means for the first/second tones. Results reveal that participants from the group 2 were significantly better than group 1, only in the late second time-window when visual cortex supposedly entrained to lip movements' activity. Significant contrasts are evidenced with stars ($p < 0.05$). (B) Mean phase distributions of the group 1 (blue) and group 2 (pink). The two separate populations were sorted based on their individual preferred phase at the second tones (blue and pink dots), where visual entrainment supposedly took place.

The ANOVA on *d'* scores revealed a significant interaction between tone position and group ($F(1, 9) = 5.893$; $p = 0.038$). Bonferroni-corrected pairwise t-tests showed that participants from the group 2 were better than the group 1 to detect the second tones ($T(1,9) = -0.786$; p

= 0.028) but not the first tones (T(1,9) = -0.208; p = 0.629). Results also replicated the effect of tone position (F(1, 9) = 7.715; p = 0.021) with greater d' for the tones sorted as second than first. Finally, no main effect of group was found (F(1, 9) = 2.103; p = 0.181). No difference between threshold (SNR_{group1} = 1.39e10^{-3} ± 2.31e10^{-3}; SNR_{group2} = 1.43e10^{-3} ± 3.47e10^{-3}; T(1, 24) = - 0.66; p = 0.95; two-tailed), nor hit rates (hit_{group1} = 0.761 ± 0.003; hit_{group2} = 0.763 ± 0.004; T(1, 24) = -0.23; p = 0.84; two-tailed) were found in the calibration task, ruling out any hearing difference.

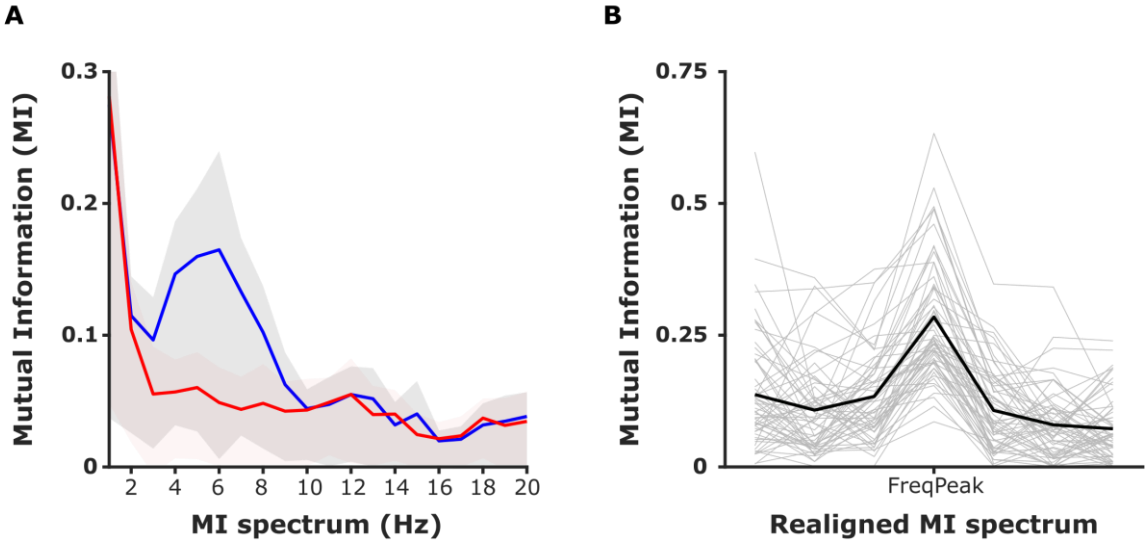

Figure S3: Mutual information between lips movements and auditory envelope in the movies. (A) Mean mutual information spectrum (± standard deviation) between the vertical aperture of the lips and the corresponding (blue line) or random (red line) speech envelope from movies. The greater dependency between the two signals is reflected by the bump localised in the theta frequency band of interest (4 - 8 Hz). (B) Realigned spectrum on the frequency with the greater MI peak (± 1-3 Hz) of each movie (grey lines) and averaged (black line). For each movie, we applied a peak detection and selected the stimuli with a greater MI between the vertical aperture of the lips and auditory envelope situated in the frequencies of interest only (i.e. 4, 5, 6, 7 and 8 Hz).